

Ferrographic Tracking of Bacterial Transport in the Field at the Narrow Channel Focus Area, Oyster, VA

W. P. JOHNSON,*† P. ZHANG,†
M. E. FULLER,‡ T. D. SCHEIBE,§
B. J. MAILLOUX,|| T. C. ONSTOTT,||
M. F. DEFLAUN,‡ S. S. HUBBARD,‡
J. RADTKE,¶ W. P. KOVACIK,° AND
W. HOLBEN°

Department of Geology and Geophysics, University of Utah, Salt Lake City, Utah 84112, Envirogen, Inc., Princeton Research Center, 4100 Quakerbridge Road, Lawrenceville, New Jersey 08648, Pacific Northwest National Laboratory, Richland, Washington 99352, Department of Geosciences, Princeton University, Princeton, New Jersey 08544, Lawrence Berkeley National Laboratory, Berkeley, California 94720, Golder Federal Associates, Inc., Atlanta, Georgia 30341, and Division of Biological Sciences, The University of Montana, Missoula, Montana 59812

The first results from an innovative bacterial tracking technique, ferrographic capture, applied to bacterial transport in groundwater are reported in this paper. Ferrographic capture was used to analyze samples during an October 1999 bacterial injection experiment at the Narrow Channel focus area of the South Oyster site, VA. Data obtained using this method showed that the timing of bacterial breakthrough was controlled by physical (hydraulic conductivity) heterogeneity in the vertical dimension as opposed to variation in sediment surface or aqueous chemical properties. Ferrographic tracking yielded results that compared well with results from other tracking techniques over a concentration range of 8 orders of magnitude and provided a low detection limit relative to most other bacterial tracking techniques. The low quantitation limit of this method (~20 cells/mL) allowed observation of transport of an adhesion-deficient bacterium over distances greater than 20 m in the fine sand aquifer underlying this site.

Introduction

Bacterial transport in the subsurface is a subject of increasing interest given the recognition of subsurface delivery of bacteria as an attractive and viable remedial option to degrade or transform contaminants (bioaugmentation) (1). Subsurface bacterial transport is also an important concern in the protection of groundwater supplies from contamination by pathogens (2, 3). Understanding bacterial transport in the

subsurface has been constrained by the lack of specificity and low resolution of existing bacterial tracking techniques (2, 4–6). The purpose of this paper is to describe the first application of an innovative bacterial tracking method, ferrographic capture, to field transport of bacteria in groundwater. The transport experiment described in this paper was performed in October 1999 as part of a larger field-scale bacterial transport study within an unconfined sandy aquifer near Oyster, VA. Bacterial transport is being studied at Oyster by a multidisciplinary research team funded by the Natural and Accelerated Bioremediation (NABIR) Program of the U.S. Department of Energy. One of the purposes of this project is to evaluate the relative importance of physical and chemical heterogeneities in controlling bacterial transport at the field scale. During the course of this study, several innovative bacterial tracking techniques have been refined or developed to support monitoring of the injected microbe. These techniques include ferrographic capture, flow cytometry, combustion IRMS and HPLC–electrospray ionization–MS of ¹³C-enriched bacteria, and quantitative polymerase chain reaction (qPCR) and they are described in detail elsewhere (4–9). Some of the above techniques as used in this study relied on a vital fluorescent protein stain, 2',7'-dichlorodihydrofluorescein diacetate/succinimidyl ester (CFDA/SE, Molecular Probes, Inc., Eugene, OR) for detection of the bacteria. Here the term "vital" refers to absence of adverse effects on cell culturability. Development and utilization of this stain is described in Fuller et al. (8, 9).

Ferrographic capture combines the selectivity of immunomagnetic tagging with the high resolution of ferrographic separation (4, 5). The technique provides selectivity due to reliance on antibody–antigen recognition to magnetically tag the bacteria of interest after sample collection. It also provides high-resolution microscopic enumeration (as low as 10 cells/mL for a 0.5-mL sample) following deposition of the magnetically tagged bacteria onto a small area (0.01 cm²) on a glass slide. In laboratory column experiments, ferrographic capture compared favorably in terms of accuracy, resolution, speed, and cost relative to the other bacterial tracking methods listed above (6). In this paper, ferrographic capture is shown to provide sufficient analytical resolution to allow recognition of the effects of subsurface heterogeneity on bacterial transport in the field and observation of transport of an adhesion-deficient bacterium over distances greater than 20 m in a fine-grained sandy aquifer. Ferrographic capture is also shown to have a low quantitation limit relative to most of the other bacterial tracking methods utilized during the October 1999 field experiment, while also providing accurate results at the highest measured cell concentrations.

Methods

Bacterial Strain. An indigenous aquifer organism was isolated from the Oyster site and designated DA001. DA001 was identified as a *Comamonas* sp. (*Comamonas*; 16S sequence similarity 0.965). An adhesion-deficient variant of DA001 was selected by a simple column assay (10) using Oyster site sediment. This adhesion-deficient variant showed 30% adhesion (70% breakthrough) to site sediment in column (70 cm long, 7.2 cm diameter) assays performed with a pore water velocity of 0.99 m/d.

Preparation of Bacteria. The inoculum was grown and labeled as described in DeFlaun et al. (6) and Fuller et al. (8, 9) to develop a bacterial suspension in which 10% of the cells were labeled with ¹³C, while 90% were stained with the vital fluorescent stain CFDA/SE. The bacterial suspension was diluted to a nominal concentration of 1E9 cells/mL in 120

* Corresponding author phone: (801)581-5033; e-mail: wjohnson@mines.utah.edu.

† University of Utah.

‡ Envirogen, Inc.

§ Pacific Northwest National Laboratory.

|| Princeton University.

‡ Lawrence Berkeley National Laboratory.

¶ Golder Federal Associates, Inc.

° The University of Montana.

L of Narrow Channel artificial groundwater (NCAGW) (6) and transported to the field. Immediately prior to injection, the bacterial suspension in NCAGW was again diluted, this time with groundwater from the Narrow Channel focus area (NCGW) to a final concentration of 1.36×10^8 cells/mL (was at 1×10^8 , do we need to replot?) in a final volume of about 800 L.

Tracking Methods. Tracking methods developed for bacterial transport experiments planned for the South Oyster site were constrained by several requirements. These requirements were in some cases dictated by the owners of the site and in other cases by the potential future use of these methods for tracking cells during actual bioaugmentation activities. The constraints imposed on bacterial injection experiments at the Oyster site required that the tracking methods adhere to the following criteria: (i) be compatible with use of an indigenous bacterial strain; (ii) cause no adverse effects on the physiology of the cells; (iii) not involve the use of radioactive or toxic compounds; (iv) cause no adverse effects on the transport characteristics of the cells; (v) be rapid and inexpensive to perform on large numbers of samples; and (vi) be capable of detecting the injected cells at low concentrations. Several bacterial tracking methods were utilized to track DA001 in the field including ferrographic capture, flow cytometry, combustion-IRMS of ^{13}C -enriched bacteria, and quantitative PCR. Results of these methods were also compared to direct microscopic counts using CFDA/SE fluorescence and plate counts.

Ferrographic capture, as related to enumeration of bacteria in natural waters, was recently developed at the University of Utah (4, 5). The method employs a Bio-Ferrograph (11), which utilizes a magnetic field with a maximum field strength across an interpolar gap to collect magnetically susceptible particles. The Bio-Ferrograph directs sample volumes through a small chamber over a glass substratum that sits over the magnetic gap, allowing efficient collection of magnetically susceptible particles. Minimal sample-apparatus contact, involving transport through about 7 cm of Teflon tubing prior to deposition onto the glass slide, minimizes loss of bacteria from suspension upstream of the deposition chamber. The effect on cell recovery of varied antibody concentration, magnetic bead concentration, processing flow rate, cell starvation, and suspended mineral colloids have been reported previously (4, 5).

Polyclonal rabbit antibodies raised to whole cells of *Comamonas* DA001 (Rockland Laboratories, Inc.) were attached to goat-anti-rabbit-coated paramagnetic beads (50 nm diameter, Miltenyi Biotec, Auburn, CA) by addition of 20 μL of stock antibody serum (31 mg/mL) and 40 μL of stock bead solution to 0.5 mL of Milli-Q water. The solution was vortexed at low speed for 15 min at room temperature. Removal of antibodies not attached to beads was performed with MACS MS⁺ separation columns (Miltenyi Biotec) using the manufacturer's protocol to give 1.0 mL of bead-antibody suspension. Prior to analysis, bacterial samples were amended with NaCl to increase ionic strength to approximately 150 mM, which is ideal for antibody conformation. The bead-antibody suspension (100 μL) was added to 0.5-mL aliquots of the aqueous bacterial suspension (groundwater samples to be analyzed) and then vortexed at lowest speed for 15 min at room temperature.

The bacteria-bead suspension was introduced to the Bio-Ferrograph at 0.008 mL/min, the flow rate determined to be the maximum that produced 100% recovery for the combination of magnetic beads and antibodies used in this study (4). Following capture, drops of mounting medium (Prolong, Molecular Probes, Inc.) were placed directly on the individual deposition areas on the glass substratum. A glass slide was then placed over the substratum, and the mounting media

was allowed to dry. Cells were enumerated by CFDA fluorescence with an epifluorescence microscope.

The accuracy of ferrographic capture was checked regularly by analyzing a standard DA001 suspension in NCAGW once for every 20 field samples that were analyzed. Selected field samples were run repeatedly over time in order to determine the effect of sample holding time on the accuracy of the method. The quantitation limit was found to be ~ 20 cells/mL, and the standard deviation of replication analyses was less than or equal to 10%, as described in the Results.

Plate count samples were agitated, serially diluted into phosphate-buffered saline, and plated in triplicate on R2A medium (Becton Dickinson, Cockeysville, MD). Plates were incubated at 30 °C for 2–3 d, at which time CFU of DA001 were enumerated and distinguished from background CFU on the basis of colony morphology.

Direct counts were performed by filtering up to 10 mL of the formaldehyde-preserved samples onto a 0.2- μm polycarbonate black filter. The amount filtered was calculated to deposit approximately 25–50 cells/grid with counting 30 grids/slide. Filters were mounted on glass slides with a drop of Slow-Fade Light antifade solution (Molecular Probes, Eugene, OR). The cells were counted by CFDA fluorescence using an epifluorescence microscope.

Enumeration of CFDA/SE-stained DA001 cells by flow cytometry was performed using a FACScan instrument (Becton-Dickinson Immunocytometry Systems, San Jose, CA). One milliliter of sample was mixed with 10 μL of a known concentration of 1.0 μm diameter carboxylate-modified TransFluorSpheres (TFS) (1.8×10^4 microspheres/ μL ; Ex 488 nm/Em 645 nm, Molecular Probes, Inc., Eugene, OR) prior to analysis. The TransFluorSpheres were used to calculate the volume of sample analyzed. All particles in a given sample were counted, with subsequent subtraction of particles that were too small and too faint to be bacterial cells or TFS.

The relationship between $\delta^{13}\text{C}$ values and numbers of bacterial cells was determined by regression of 10-fold serial dilutions of known cell densities (based on direct microscopic enumeration) of $\delta^{13}\text{C}$ -enriched cells ranging in concentration from 10^8 to 0 cells/mL in a total volume of 50 mL of site groundwater. This approach provided a dilution series of isotopically enriched cells against the natural bacterial population existing in the groundwater of the bacterial transport site. These samples were prepared and analyzed for stable isotope composition as described previously (7), except that a second-order polynomial regression provided the best fit of the $\delta^{13}\text{C}$ values to known numbers of cells.

For qPCR analyses, the relationship between known number of cells and the amount of specific PCR product produced was determined. A regression analysis was performed based on serially diluted numbers of target cells and a fixed amount of competitor DNA. First, a dilution series of linearized competitor plasmid DNA was amplified alone to determine the linear range of detection and quantification of PCR product on ethidium bromide-stained agarose gels. The competitor DNA concentration corresponding to the midpoint of the linear range was then selected as the fixed amount of competitor for the regression analysis of known cell numbers, as well as analysis of samples with unknown numbers of cells.

Site Description

Physical and Chemical Characteristics. The South Oyster site is located on the southern Delmarva Peninsula situated on the eastern coast of the United States between the Chesapeake Bay and the Atlantic Ocean. The surficial unconfined aquifer underlying the study area is comprised by unconsolidated to weakly cemented, well-sorted, medium- to fine-grained sands and pebbly sands (12). A fine-grained muddy silt layer at about 10 m depth below the surface (~ 7

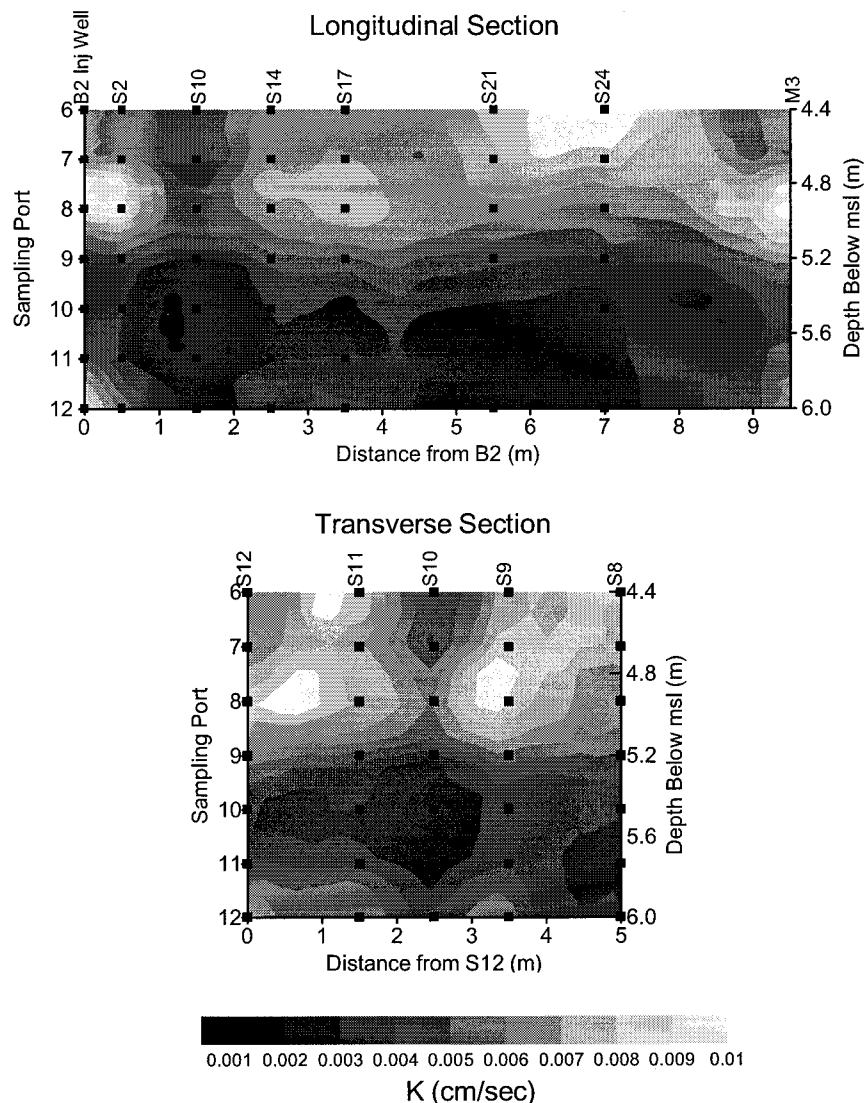


FIGURE 1. Estimated means of hydraulic conductivity probability density functions parallel (top) to the nominal flow axis and transverse (bottom) to flow (14). Numbers at the top of the sections correspond to wells and MLS locations (shown in Figure 2) and described in the Flow Cell section of the text. A higher hydraulic conductivity (K) layer is indicated about 4.5–5 m below MSL (e.g., port 8) in both sections; however, this layer is indicated to have decreased hydraulic conductivity at the location of MLS 10 in the flow axis. Higher hydraulic conductivity is also indicated at the bottom layer of the aquifer in the transverse section.

m below mean sea level, MSL) at the Narrow Channel focus area serves as a lower boundary of the surficial aquifer. The sediments comprising the surficial aquifer at the site are composed of quartz, feldspar, clays, and iron and aluminum hydroxides in decreasing order of abundance as determined by observation under a petrographic microscope (12). The clays (illite/smectite) and metal hydroxides tend to occur as coatings on the fine-grained quartz and feldspars, with the metal hydroxides comprising between 0.4% and 1.2% of the mineralogy (determined by examination under petrographic microscope) in the finer grained sediments. In contrast, the coarser grained quartz and feldspar show much lower amounts of the clay and metal hydroxide coatings (12).

The Narrow Channel focus area has been extensively characterized using hydrological, geological, and geophysical methods. The geophysical analyses performed at this site include surface ground penetrating radar (GPR) surveys, tomographic radar measurements, tomographic seismic surveys, cone penetrometer tests (CPT), and borehole flowmeter measurements. The mechanics of each of these sampling methods are described by Hubbard et al. (13), who also present an analysis of the bacterial breakthrough data. The geophysical data reveal that the geologic structure in

the Narrow Channel flow cell is simple with small undulations on otherwise gently downgradient dipping surfaces. Radar tomographic data was used as a supplement to the flowmeter data in order to obtain detailed estimates of log-conductivity probability distribution function at each location along tomographic transects (14). The estimated means of the hydraulic conductivity probability distribution functions (Figure 1) indicate that a relatively high permeability zone exists at a depth of approximately 4.5–5 m below MSL within the Narrow Channel flow cell (described below).

Water chemistry of the Narrow Channel focus area is constant with location but shows variation with depth. Aerobic subsurface conditions are displayed at most depths in the surficial aquifer at this location; however increased pH, ionic strength, and dissolved organic carbon are observed along with decreased dissolved oxygen and nitrate at the lower boundary of the aquifer at the depth of port 12 (16).

Flow Cell. The design of the Narrow Channel flow cell (Figure 2) was based on the hydrogeologic characteristics of the site (15). The flow cell is bordered on the downgradient end by groundwater extraction wells (A3, B3, and C3), which are screened over the lower 6 m of the surficial aquifer (~1–7 m below MSL). The extraction wells within the flow cell were

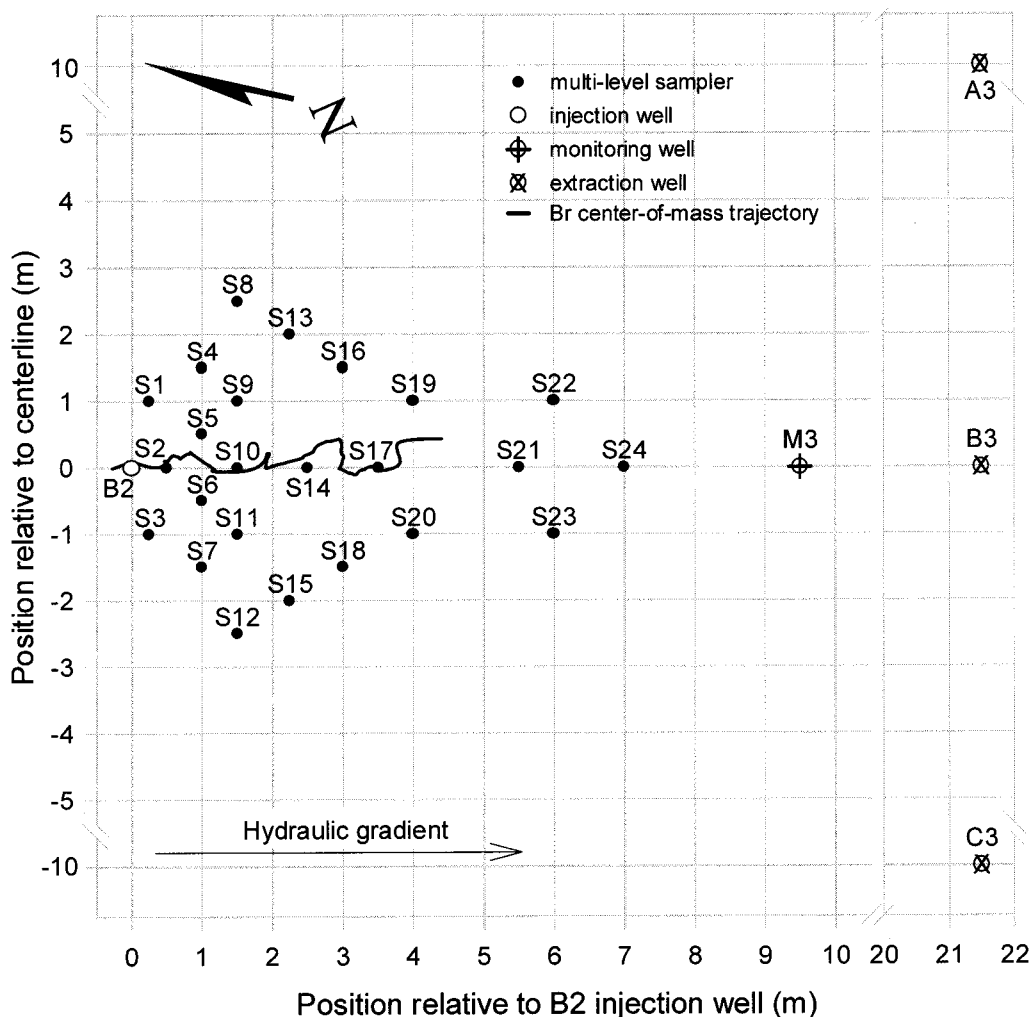


FIGURE 2. Flow cell configuration for Narrow Channel. Injection well (B2), extraction wells (A3, B3, and C3), and a tomography well (M3) are differentiated by symbols. Multilevel samplers (MLS 1–24) are also indicated; however, this paper examines breakthrough at the far-field MLS and wells (MLS 21–24, M3, and B3). Also shown is the center of mass of the injected bromide plume as tracked during the field experiment. The bromide plume trajectory indicates that flow was skewed slightly away from the nominal flow axis toward MLS 22.

used to set up a steady-state flow field prior to and during the injection experiments (15). Although injection wells exist on the upgradient border of the site (A1, B1, and C1), they were not used to set the steady-state flow field. The tracer and bacterial injection well within the flow cell is well B2, which is located 20 m upgradient from the closest (center) groundwater extraction well (B3). Within the flow cell are 24 custom-made multilevel samplers (MLS) (Figure 2) installed between the injection and extraction wells. Each MLS has 12 sampling ports vertically spaced approximately 27.9 cm apart within the lower 3 m of the surficial aquifer (lowest six evenly spaced between 4.4 and 6.2 m below MSL).

The MLS consist of a 3-cm-diameter PVC rod separated into 12 equally spaced sections that are separated by neoprene baffles and which contain one mounted sampling port. The sampling ports are 2.5 cm diameter by 16 cm long 10-slot PVC screen. Stiff polyethylene tubing (3.2 mm i.d.) runs from approximately 0.5 m above ground surface to each sampling port. An additional monitoring well (M3) is located 10 m downgradient of the tracer injection well and is screened over the lower 6 m of the surficial aquifer.

Boreholes were drilled using a roto sonic drilling method that minimized disturbance to the sediment structure. A capped casing was advanced into the formation by vibration. The MLS was inserted into the casing, and the casing cap at the bottom was detached. The casing was removed from the

formation, and the formation collapsed back in and around the MLS ports and neoprene baffles, creating direct contact between the ports and the formation. These sands are known to readily collapse into open borehole based on poor core retrieval at other site locations using conventional drilling methods. The MLS were installed during May 1999.

Field Experimental Protocol

Injection. Prior to injection, a forced hydraulic gradient was established by pumping at downgradient wells A3, B3, and C3 at rates of 20, 40, and 20 L/min, respectively, to maintain an average site pore water velocity of about 1 m/d. The pore water velocities were higher and lower than this average value at wells proximal and distal to the injection well, respectively. The flow cell was oriented with its main axis parallel to the natural flow direction as inferred from water level observations prior to installation. However, field observations of bromide transport suggest that the average flow direction under the combined natural and forced gradients was slightly to the east of the cell axis, such that flow downgradient from B2 was directed toward the area between MLS 22 and MLS 24 rather than directly to MLS 24. This suggestion was confirmed by preliminary estimates of the movement of the center of mass of the bromide plume during the experiment, made by coarse (nearest-neighbor) interpolation of vertically averaged concentration observations at the multi-level

samplers to a regular grid (see Figure 2). The skew in flow direction could result from either apparent anisotropy in hydraulic conductivity caused by preferential orientation of local heterogeneities or a change in the direction of the natural gradient from that inferred previously (or a combination of both effects). The hydraulic conductivity estimates indicate higher hydraulic conductivity values lateral to the flow axis at the depth of port 8 (~5 m below MSL) (Figure 1), consistent with the observed movement of the bromide center of mass toward MLS 22 (Figure 2).

DA001 and bromide (100 mg/L) were injected simultaneously into the flow cell over a 0.5-m interval centered at a depth of 5.0 m below MSL, corresponding to the vertical interval between ports 8 and 9 in the high permeability zone (Figure 1). The injection zone was isolated with packers, and the overall 5 L/min injection rate into B2 included injection at 1 L/min of the bacteria-bromide suspension within the isolated zone, and injection at 4 L/min of NCGW above the isolated zone (15). No injection occurred below the isolated zone (below port 9). The injection was performed over a 12-h period starting October 29, 1999, at 5:35 p.m. Pumping from the extraction wells ceased 9 days later (on November 7, 1999, at 16:15 h), after which time the hydraulic gradient relaxed to its natural value, corresponding to a pore water velocity of approximately 0.1 m/day. Daily and then weekly sampling of far-field wells M3 and B3 commenced after shutdown of the extraction wells. Sampling of port 9 in select MLS (MLS 2, 9, 11, 14, 19, 20, and 21) was continued after shutdown. Ferrographic capture was used to analyze the late-time samples in order to determine whether extended tailing of the elution portion of the breakthrough curve was significant, since this would indicate slow detachment of cells from the sediment.

Sampling. A custom manifold was developed to apply continuous suction to all sampled ports simultaneously using a peristaltic pump. All ports were pumped continuously and equally in order to minimize inducement of a vertical hydraulic gradient between the ports. The manifold was based on a design by Hitchman (17), but with alterations to facilitate sampling. The manifold was developed from a 100-mL plastic syringe into which tubing from the 12 ports and the peristaltic pump had been tapped and sealed using a silicon sealant. Valves upstream of the manifold directed the water into either a sample vial or into the manifold, which then emptied into a disposal tank. Prior to sample collection, 50 mL of groundwater was collected and then discarded to flush the tubes connected to the sample vials between sampling events. The manifold was pumped such that each sampling port flowed continuously at a rate of 4 mL/min, which allowed the tubing to be flushed while minimizing the impact on the flow field.

Sampling strategies concerning timing and intensity of sampling at each well were developed from forward numerical modeling of the injection experiment (15). Samples were taken from only the lower eight ports (ports 5–12) since numerical models suggested that the upper four ports would be unlikely to show bacterial breakthrough under the given injection protocol. Following collection, samples were preserved and shipped according to the needs of each analysis. One split (50 mL) was stored at 4 °C and shipped frozen on ice to the University of Montana for qPCR and ¹³C/IRMS analyses. A second split (15 mL) was preserved with formaldehyde (1% final concentration; v:v), stored at 4 °C, and shipped cooled (unfrozen) on ice to the University of Utah for ferrographic tracking. A third split (35 mL) was preserved with formaldehyde, stored at 4 °C, and shipped cooled on ice to Envirogen, Inc. and Princeton University for direct counts of CFDA/SE-stained cells and flow cytometry. An unpreserved sample was also stored at 4 °C and shipped cooled on ice to Envirogen, Inc. to determine the number of

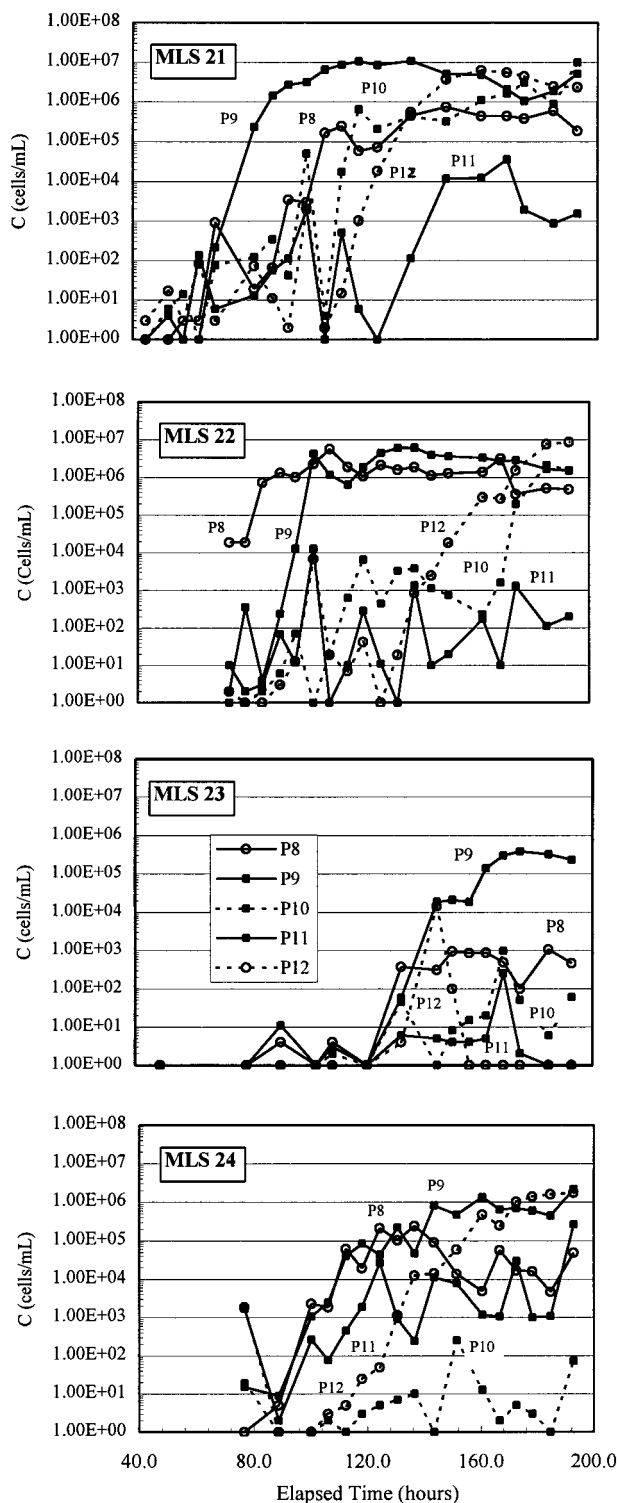


FIGURE 3. Breakthrough curves for bacteria in MLS 21–24 for ports that showed significant breakthrough concentrations, e.g., ports 8–12 (P8–P12 on the figure). Symbols and lines used to differentiate ports are given in legend of MLS 23 on the figure. Elapsed time represents time elapsed since the start of the injection. Observed cell concentration (*C*, cells/mL) is given on the ordinate axis.

culturable cells (CFU) and bromide concentration. Bromide measurements were made with an ion-specific probe (Cole-Palmer 27502-05, Vernon Hills, IL). The detection limit for bromide was 0.5 mg/L, with a standard deviation of replicate analyses of 0.2 mg/L.

Approximately 800 field samples were analyzed by ferrographic capture over the course of 1 month. The samples

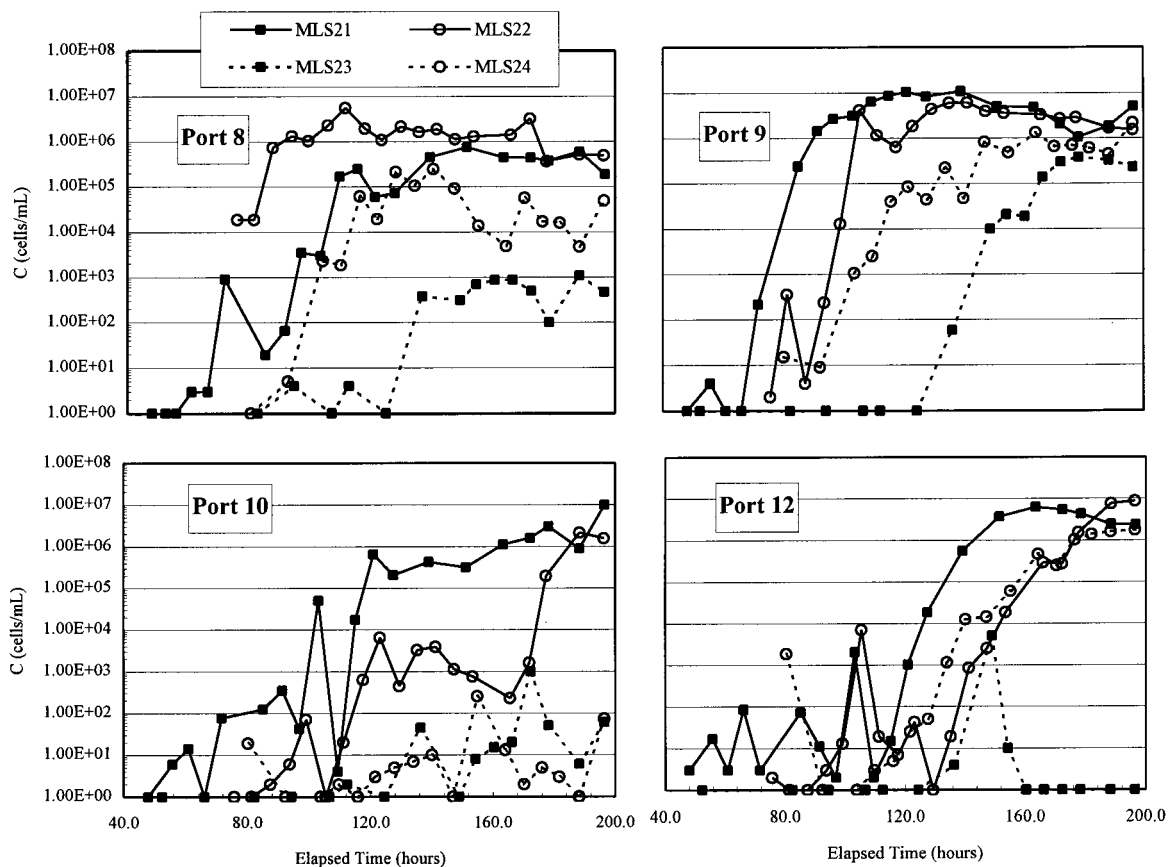


FIGURE 4. Bacterial breakthrough curves arranged according to port for MLS 21–24. Figure specifics are equivalent to Figure 3.

analyzed for cell breakthrough were obtained from the wells farthest downgradient in the flow field (MLS 21–24, M3, and B3), since ferrographic capture was amenable to analysis of low cell concentrations in the field.

Results and Discussion

Bacterial Breakthrough in MLS 21–24. Breakthrough of bacteria was clearly observed in, and occurred earliest and to the highest concentrations in, ports 8 and 9 for all of the far-field MLS (Figure 3), as would be expected since injection occurred between the levels of port 8 and port 9. Some ports (10–12) showed breakthrough in only some of the wells, whereas other ports showed no breakthrough (ports 5–7). The variations in the data at cell concentrations below a few thousand cells per milliliter were caused by sample mixing in the vacuum manifold during collection. The operation sequence for valves upstream of the manifold was sufficiently complex that small volumes of groundwater in the manifold were occasionally drawn into the sample vials, thereby causing cross-contamination. This is observed from the increase in cell counts in all ports following breakthrough in any port. For example, in MLS 23 the cell counts in all ports rise after breakthrough in port 9 at 120 h. MLS 21 ports 8, 10, and 12 also show increased but highly variable cell counts after breakthrough in port 9 at 60 h. Actual breakthrough in ports 8, 10, and 12 occurred much later than breakthrough in port 9 in MLS 21, observed as a rise in cell concentration to a steady-state breakthrough plateau (Figure 3). The different timing and extent of breakthrough among the ports at these higher cell concentrations indicates that vertical mixing between the sampling ports was not significant. The low concentration cross-contamination was not due to laboratory contamination since quality control standards in this concentration range showed steady expected values (described below).

Notable is the very high relative concentration achieved (e.g., $C/C_0 \sim 0.1$, or only 90% attachment) at distances as far as 5 m from the source in this fine sand aquifer. A one-dimensional model of bacterial transport was previously developed and used to extrapolate expected bacterial concentrations observed in laboratory experiments on 50-cm intact cores to larger transport distances for the purpose of experimental design (15). Under even optimistic assumptions of attachment rates from the core experiments, the model predicted that over 96% of the bacteria would attach within the first 2 m of transport and that bacterial concentrations would be undetectable at distances greater than 5 m. The contrast between the model prediction and field observations at distances greater than 5 m suggests that transport of bacteria at the field scale was enhanced by processes that did not operate at the core scale.

Vertical Distribution of Bacterial Breakthrough (Ports 8–12). The time to breakthrough in a given port was generally directly related to distance of the MLS from the source and the flow axis (Figure 4). For example, increasing time to breakthrough in port 9 follows the order MLS 21, 22, 24, and 23, and increasing breakthrough concentration (maximum observed concentration) in this port follows the order MLS 23, 24, 22, 21. MLS 21 shows the earliest breakthrough and highest concentrations since it is on the flow axis and is closest to the source. MLS 22 shows the second-earliest breakthrough and second highest concentrations since it is on or close to the flow axis and is downgradient of MLS 21 but upgradient of MLS 24. MLS 23 is upgradient of MLS 24 but is farther from the flow axis than all of the other wells. Transport of bacteria to MLS 23 can be expected to involve diminished advection relative to the other wells, and so MLS 23 showed the latest breakthrough at the lowest concentrations of the four far-field MLS (Figures 3 and 4). Correspondence of the timing of peak breakthrough and peak

breakthrough concentration in a given MLS to distance from the source and flow axis indicates that the site is relatively homogeneous in the lateral dimension (as opposed to the vertical dimension). An exception to the above trends is port 8, which shows earlier breakthrough in MLS 22 relative to MLS 21 despite the downgradient position of MLS 22 relative to MLS 21. This may be due to the above-described higher hydraulic conductivity indicated (Figure 1) lateral to the flow axis at the depth of port 8.

Differential breakthrough among the ports above and below the levels of ports 8 and 9 would be expected due to the injection having taken place between the level of ports 8 and 9. That is, dispersion would necessarily be a significant component of transport of cells from the depth of ports 8 and 9 to other depths (other ports), and so later breakthrough times and lower breakthrough concentrations would be expected in ports 10–12. However, in some wells the observed breakthrough concentration in port 12 was higher, and in some cases breakthrough in that port was earlier relative to ports 11 and 10, indicating that vertical variations in parameters such as hydraulic conductivity, water chemistry, and/or sediment chemistry significantly affected transport. To determine the potential effects of water and sediment chemistry on the timing of bacterial breakthrough, a comparison of bacterial and bromide breakthrough was made, as described below.

Bacterial Breakthrough Relative to Bromide. Bromide breakthrough was observed in all ports that showed bacterial breakthrough. Breakthrough of DA001 relative to bromide showed that no significant retardation of mobile DA001 occurred during transport (e.g., ports 9 and 12, Figure 5). This result indicates that the timing of breakthrough of the mobile bacterial population was not significantly affected by interaction with the sediment. Hence, physical heterogeneity rather than solution or sediment chemical heterogeneity governed the earlier breakthrough of DA001 in port 12 relative to ports 11 and 10 that was observed in some MLS (Figure 3). A higher hydraulic conductivity layer was indeed indicated at the lowest depths of the flow cell (Figure 1). Bacteria and bromide injected into the isolated zone between ports 8 and 9 may have been advected to the deeper high hydraulic conductivity zone due to lack of injection below the isolated zone.

Bromide and bacterial breakthrough concentrations were lower in a given port for MLS located farther from the source and the flow axis due to dispersion decreasing these aqueous concentrations during transport. In addition to dispersion, however, bacteria experienced attachment to the subsurface media. Observed C/C_0 values for bacteria were increasingly lower than those for bromide in a given port for MLS located farther from the source and the flow axis (Figure 5), consistent with filtration of cells during transport. Note that the bromide breakthrough curves for MLS 22 relative to MLS 23 (Figure 5) also indicate skew of the plume toward MLS 22.

The greater C/C_0 observed for DA001 relative to bromide in the ascending limb of the breakthrough curve for port 12 of MLS 22 may indicate faster advection of DA001 relative to bromide; however, the breakthrough curves are not sufficiently complete to make this determination. Differential advection of DA001 relative to bromide was observed in all laboratory intact core experiments (12). A discussion of differential advection of DA001 versus bromide during transport at this site as reflected in data from the near-field wells is in preparation.

Bacterial Breakthrough in Far-Field and Extended Tailing. Bacterial breakthrough in wells M3 and B3 (Figure 6) indicate that DA001 achieved distances of transport greater than 20 m in this fine sand aquifer. The low concentrations observed in M3 (peak $\sim 1E4$ cells/mL) and B3 (~ 500 cells/mL) relative to the concentrations observed in upgradient

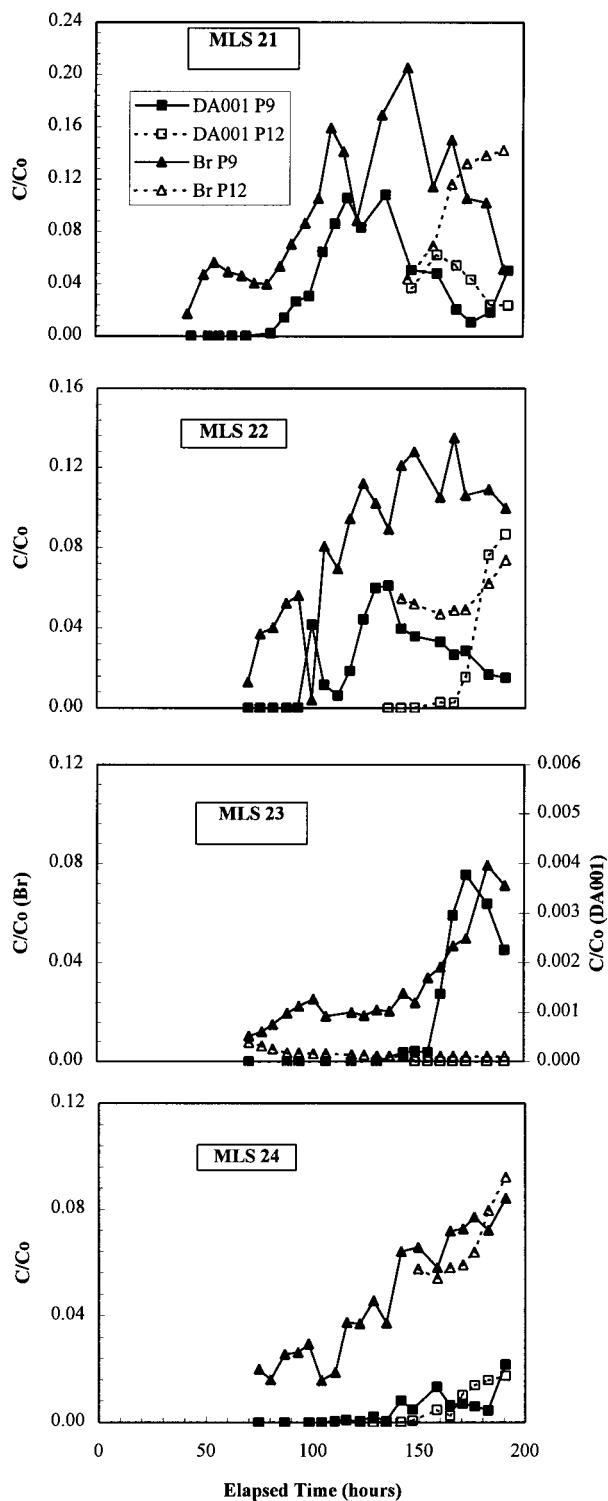


FIGURE 5. Bromide and bacterial breakthrough curves from MLS 21–24 ports 9 and 12 (P9 and P12). Relative concentration (C/C_0) is used on the ordinate axis where C_0 represents the injected concentration of bacteria (DA001) or bromide (Br).

MLS are due not only to attenuation during transport but also to dilution during sampling of these wells, which are screened over a 6 m depth. The forced-gradient pore water velocity of ~ 1 m/d implemented for 9 d was followed by a natural-gradient pore water velocity of ~ 0.1 m/d. One would therefore expect nominal breakthrough times of ~ 5 – 6 d for MLS 21 (5.5 m at 1 m/d), ~ 14 d for M3 (9 m at 1 m/d plus 0.5 m at 0.1 m/d), and ~ 120 d for B3 (9 m at 1 m/d plus 11 m at 0.1 m/d). These values are consistent with the observed

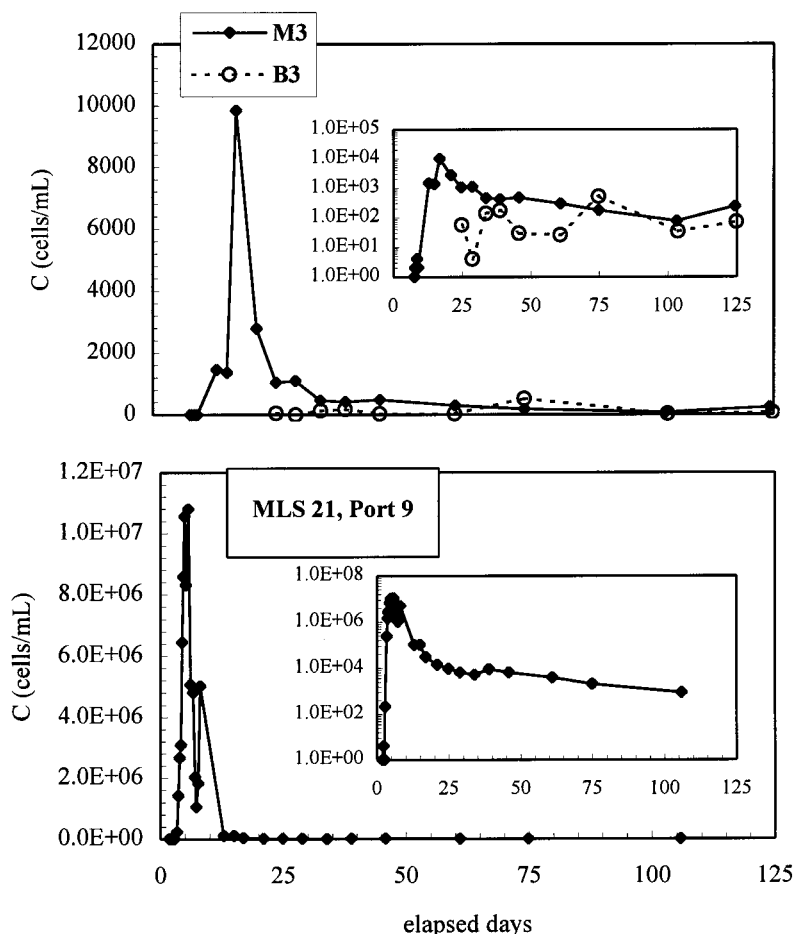


FIGURE 6. Bacterial breakthrough at wells M3 and B3 (top). Cell concentration (cells/mL) is given on the ordinate axis and is shown in both linear and log (inset) scales. Extended tailing of bacterial concentrations over time is shown in port 9 of MLS 21 (bottom).

timing of peak breakthrough in these wells, although the timing of breakthrough at B3 is unclear due to the low observed concentrations.

Also shown in Figure 6 is extended tailing of relatively low cell counts in port 9 of MLS 21, indicating that a significant fraction of the attached population detached over the time period following injection. The kinetics of bacterial attachment and detachment will be modeled and compared to the extended tailing data from multiple MLS to determine the mass of bacteria that detached over longer time periods relative to the mass of bacteria that were attached immediately following breakthrough. This determination, in addition to forward transport modeling based on the observed attachment–detachment kinetics, will help to determine whether detachment may be significant in bacterial transport over longer time periods.

Comparison to Other Bacterial Tracking Methods.

Ferrographic capture yielded results that compared favorably with the other bacterial tracking methods employed in the study, as shown for example by the results from port 9 in MLS 21 and 24 (Figure 7). Ferrographic capture appeared to provide the lowest quantitation limit assuming that the steep slope of the bacterial breakthrough curve observed at higher concentrations (e.g., between 1E4 and 1E5 cells/mL) should continue to lower concentrations. With this assumption, one can estimate the quantitation limit for a given method based on the concentration at which the slope becomes significantly less steep as the concentration decreases. Applying this criteria to the data from port 9 (Figure 7), it appears that the quantitation limit (cells/mL) for direct counting and qPCR was about 1E4, that for plate counting (CFU) was 1E3, and that for flow cytometry was about 1E3. The quantitation limit

for ^{13}C -IRMS appears to have been between 1E2 and 1E1 cells/mL and that for ferrographic capture appears to have been around 1E1 cells/mL, which is expected from previous laboratory studies. At higher cell counts, ferrographic capture, direct count, and flow cytometry agree extremely well, showing rapid variations in concentration that the three methods corroborate as being real but which may or may not represent variations in actual subsurface breakthrough. These variations were not reflected in the qPCR and ^{13}C -IRMS data. However, this does not indicate lack of sensitivity of those two methods since the samples for these two methods were collected in a 50-mL vial directly before, but separately from, collection of the 50-mL vial analyzed by the other methods.

That the cells did not grow during transport is indicated by the fact that the stain in the cells was not diluted with transport. Flow cytometry indicated a constant fluorescence per cell with distance traveled (between ports) and with time (within a given port). The fact that the ^{13}C analysis agrees with the other methods indicates that cell lysis was not significant during transport since the other methods would not have detected lysed cells. The good agreement between the methods resulted from the relative specificity of each method for DA001 since identification was by fluorescence, $\delta^{13}\text{C}$, DNA, or distinct colony morphology.

Quality Control. Standards comprised by two different cell suspensions in NCAGW were used over two different time periods to check the accuracy of ferrographic capture over time. Changes in cell counts for these artificial standards would indicate loss of activity of the antibodies or degradation of the magnetic microspheres used in the method. Consistent cell counts were achieved over time (Figure 8), with a

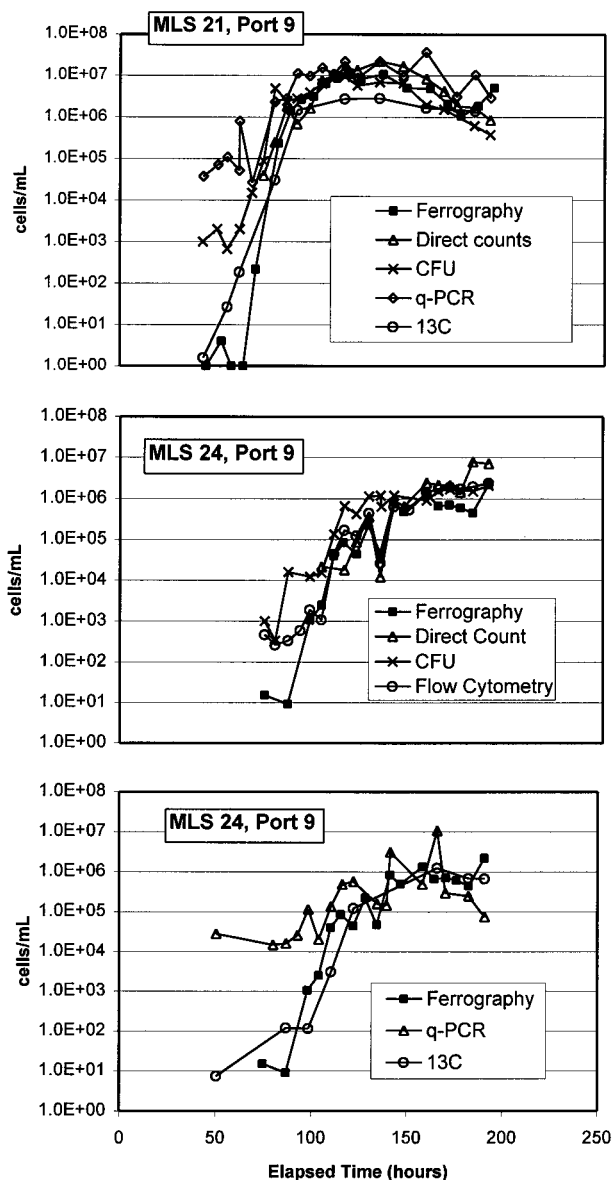


FIGURE 7. Bacterial breakthrough curves in MLS 21 and MLS 24, port 9 for the various methods utilized to track bacterial concentrations during the October 1999 field experiment. Ferrographic capture (ferrography), direct counts, plate culturing (CFU), quantitative PCR (q-PCR), ¹³C IRMS (13C), and flow cytometry all compare favorably with different apparent detection limits for the various methods indicated by horizontality of the breakthrough curve during initial breakthrough.

deviation of 10% and 6% around a mean of 623 and 743 cells/mL, respectively. Field standards (collected on November 1, 1999, at 11:45 a.m. from MLS 21 ports 8 and 7) showed monotonic decreases in cell recovery over long periods of time. The results indicate that cell counts decreased by about a factor of 2 over a 2-month period. This decrease may have been due either to loss of CFDA stain from the bacteria with time or due to changes in bacterial antigen structure with time. Experiments are presently being performed to determine the cause of this decrease, and preliminary results indicate that the decrease is due to the presence of the fixing agent (formaldehyde). All samples in this study were analyzed within a 30-d period to minimize decreases in cell counts, and given the very good agreement between ferrographic and other analyses employed in the study, it is concluded that analysis within a 30-d period is sufficient to yield excellent results.

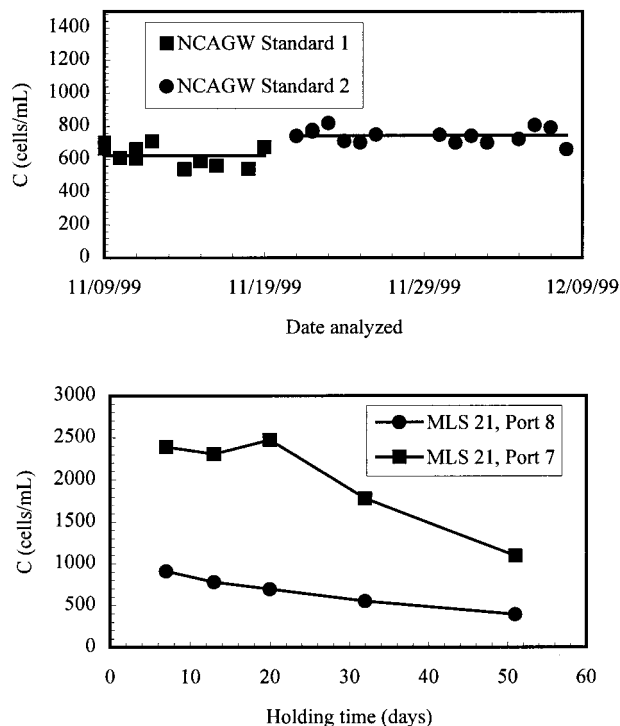


FIGURE 8. Standard concentrations of DA001 in narrow channel artificial groundwater (NCAGW) monitored repeatedly during the period that the analyses were performed. The data show low deviation around measured concentrations (top), indicating that antibody and magnetic bead activities remained constant over the course of the analyses. Stored field samples monitored repeatedly over time (MLS 21 ports 7 and 8) indicate decreased efficiency of cell recovery at a rate of about 50% per 50 d. Samples analyzed using ferrographic capture were run within 30 d of receipt.

Acknowledgments

The investigators acknowledge the support of the U.S. Department of Energy (DOE), Natural and Accelerated Bioremediation Research Program (NABIR)—Acceleration Element (Grant DE-FG03-99ER62820/A000). The authors thank Drs. Keun-Hyung Choi and Fred Dobbs at Old Dominion University for providing samples following the initial 200-h phase of the experiment. The authors acknowledge the leadership of Dr. Frank Wobber, the Program Manager for the Acceleration Element of NABIR. Access to the field site was granted by The Nature Conservancy, Virginia Coast Reserve. We also acknowledge the excellent work of Phil Gardner, Aaron Norton, David Stone, Tiffany Copyak, and the rest of team FASTBUGS (Ferrographic Analysis in Short Time By Under-Graduate Students). We appreciate the hard work of an anonymous reviewer in improving this manuscript.

Literature Cited

- Steffan, R. J.; Sperry, K. L.; Walsh, M. T.; Vainberg, S.; Condee, C. W. *Environ. Sci. Technol.* **1999**, *33*, 2771–2781.
- Harvey R. W. *FEMS Microbiol. Rev.* **1997**, *20*, 461–472.
- Harvey R. W. In *Manual of Environmental Microbiology*; Hurst, C. J., Knudsen, G. R., McInerney, M. J., Stetzenback, L. D., Walter, M. V., Eds.; ASM Press: Washington, DC, 1997; pp 586–599.
- Zhang, P.; Johnson, W. P.; Rowland, R. *Environ. Sci. Technol.* **1999**, *33* (14), 2456–2460.
- Zhang, P.; Johnson, W. P. *J. Magn. Magn. Mater.* **1999**, *194* (1–3), 267–274.
- DeFlaun, M. F.; Fuller, M. E.; Johnson, W. P.; Zhang, P.; Mailloux, B. J.; Onstott, T. C.; Holben W.; Balkwill, D.; White, D. Comparison of innovative methods for monitoring bacterial transport. *Environ. Sci. Technol.* (submitted for publication).

- (7) Holben, W. E.; Ostrom, P. H. Monitoring bacterial transport by stable isotope enrichment of cells. *Appl. Environ. Microb.* (in press).
- (8) Fuller, M.; Streger, S.; Rothmel, R.; Mailloux, B.; Onstott, T. C.; Fredrickson, J.; Balkwill, D.; DeFlaun, M. Development of a vital fluorescent staining method for monitoring bacterial transport in subsurface environments. *Appl. Environ. Microb.* (in press).
- (9) Fuller, M.; Mailloux, B.; Zhang, P.; Vainberg, S.; Johnson, W. P.; Onstott, T. C.; DeFlaun, M. F. Evaluation of CFDA/SE-staining coupled with multiple detection methods during a field-scale bacterial transport experiment. *Environ. Sci. Technol.* (submitted for publication).
- (10) DeFlaun, M. F.; Tanzer, A.; McAteer, A.; Marshall, B.; Levy, S. *Appl. Environ. Microbiol.* **1990**, *56* (1), 112–119.
- (11) Seifert, W. W.; Westcott, V. C.; Desjardins, J. B. U.S. Patent No. 5714059, 1998.
- (12) Dong, H.; Onstott, T. C.; DeFlaun, M. F.; Fuller, M. E.; Streger, S. H.; Rothmel, R. K.; Mailloux, B. J. Transport of adhesion deficient bacteria in heterogeneous porous media: relative dominance of physical vs chemical control on bacterial transport. *Environ. Sci. Technol.* (submitted for publication).
- (13) Hubbard, S.; Chen, J.; Peterson, J.; Majer, E.; Rubin, Y.; Williams, K.; and Swift D. Hydrogeophysical characterization of the Oyster bacterial transport site using geophysical data. *Water Resour. Res.* (submitted for publication).
- (14) Chen, J.; Rubin, Y.; Hubbard, S. Estimating hydraulic conductivity at the Oyster bacterial transport site using Bayesian statistics. *Water Resour. Res.* (submitted for publication).
- (15) Scheibe, T. D.; Chien, Y.; Radtke, J. Use of quantitative models to design microbial transport experiments in a sandy aquifer. *Ground Water.* (submitted for publication).
- (16) Mailloux, B. J.; Fuller, M.; Onstott, T. C.; Hall, J.; Dong, H.; Beavis, A.; DeFlaun, M. F.; Streger, S.; Rothmel, R.; Green, M.; Swift, D. J. P.; Griffin, T.; Hubbard, S.; Chen, J. The role of physical heterogeneity on the field-scale transport and attachment of bacteria. *Water Resour. Res.* (submitted for publication).
- (17) Hitchman, S. P. *Ground Water* **1988**, *26* (3), 348–349.

Received for review April 7, 2000. Revised manuscript received October 4, 2000. Accepted October 23, 2000.

ES001170E